On the Possibility of Observing Transverse Echos in RHIC

O. Brüning,* W. Fischer and B. Parker

October 29, 1999

Abstract

Echo phenomena are well known in plasma physics and have been observed in accelerators in the longitudinal plane. Echo measurements are appealing since they allow the determination of small diffusion coefficients in a relatively short time. In this paper we explore the possibility of observing transverse echos in an accelerator. The easiest way to create a transverse echo is to apply a dipole kick to the beam, followed by a quadrupole kick. The technical challenge lies in the application of the quadrupole kick. We consider two approaches for the quadrupole kick: a pulsed quadrupole that is excited for a few turns and an AC quadrupole that is excited for a couple of hundred turns. For both cases simulations are performed and the technical feasibility is investigated.

1 Introduction

Echo phenomena are well known in plasma physics [1]. However, the effect has only been recently introduced into accelerator physics and first measurements of longitudinal echo signals suggest the possibility of using this technique for beam diagnostics [2–8].

The echo signal is an interference pattern of two consecutive kicks of different harmonics. It can appear at a time long after the initial signal has disappeared due to filamentation in phase space. The echo signal shows on a harmonic which is equal to the difference of the harmonics associated with the two consecutive kicks. For example, applying a dipole kick followed by a quadrupole kick results in a dipole echo signal [3]. In the following we investigate only this case.

A particularly interesting aspect of echo measurements is the possibility of diffusion coefficient measurements in short time intervals since any form of diffusion reduces the echo signal. While such measurements are desirable for the longitudinal and transverse particle motion, only longitudinal echo signals have been measured so far [5,7,8].

One reason for the lack of transverse echo measurements is the difficulty of applying a short quadrupole kick to the beam. Most quadrupoles have inductances large enough to limit the change of the quadrupole field to time scales of several hundred turns. The theory developed in references [2] and [3] requires, however, a kick of less than one turn in duration.

In this note we study two different operational modes of the quadrupole:

- A pulsed quadrupole excitation of at least 1 turn but no longer than 10 turns.
- An AC-quadrupole excitation over a couple of hundred turns.

---

*Home institute CERN, Geneva, Switzerland.

Table 1: RHIC machine parameters used in the simulations.

Parameter	Symbol	Unit	Value
Revolution frequency	f_{rev}	kHz	78.196
Particle momentum	p	GeV/c	25
Maximum transverse rms beam size	$\sigma_{x,y}$	mm	2.42
Maximum transverse β-function in arcs	$\beta_{x,y}$	m	48.6
Transverse tune	$Q_{x,y}$	1	28.19/29.18
Detuning with action	$\partial Q_{x,y}/\partial J_{x,y}$	m^{-1}	1500

For all simulations we used the RHIC injection parameters for proton operation (see Tab. 1, cf. Ref. [9]). At injection the quadrupole kick will show the strongest effect. Proton operation is preferable compared to gold operation since the effect of intrabeam scattering, which may reduce the echo signal to undetectable levels, is less severe.

In the following sections we first present numerical simulations for both cases of quadrupole operation. We then discuss the technical options of implementing these cases in RHIC.

2 Simulation Model

We simulate the motion of particles in a distribution as they travel around the ring for a number of turns. We observe the dipole moment of the distribution and its rms value over time.

The simulations are done in a four dimensional phase space including nonlinear detuning with amplitude, linear coupling and noise. The simulation uses four linear transfer maps (see Fig. 1). The first map adjusts the desired fractional tune and includes the effect of tune modulation. The other four transfer maps have the desired phase advances between consecutive octupole and skew quadrupole kicks. We assume that the maximum β-function is reached at the location of the dipole and quadrupole kick.

Nonlinearity of the particle motion is introduced by three octupole kicks placed $\pi/2$ and $\pi/4$ apart in order to cancel the first order resonance driving terms. Linear coupling is introduced by two skew quadrupole kicks spaced $\pi/2$ apart in order to cancel the excitation of the sum resonance. The effective coupling is measured with an FFT of the transverse particle motion. The quadrupole kicks are applied in thin lens approximation over a variable number of turns at the end of the above sequence of transfer maps and octupole and skew quadrupole kicks. For a kick length larger than one turn we assume that the signal envelope follows a triangle shape where the magnet is ramped up and down. Noise is modeled by applying a random transverse kick.

In all cases shown here we consider a distribution of 10,000 particles. The evolution of its dipole moment and rms value are observables in a beam experiment. The initial particle distribution is Gaussian in the action variables and uniform in the angel variables. The dipole kick is introduced by an offset of the distribution in the horizontal plane (see Fig. 2). We assume a normalized integrated quadrupole strength k of
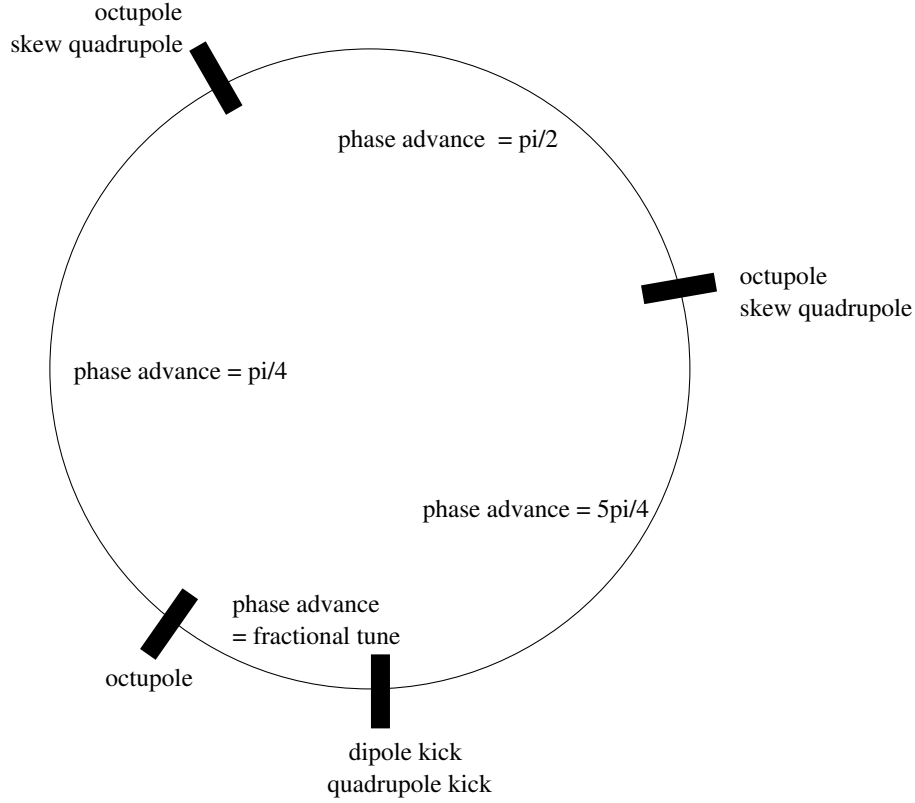
Figure 1: Model of RHIC that is used in the numerical simulations.

$$1.0 \cdot 10^{-4} \mathrm{m}^{-1} \leq \mathrm{k} \leq 2.0 \cdot 10^{-3} \mathrm{m}^{-1}. \tag{1}$$

k is given by

$$k = \int_l \frac{eg}{p} \mathrm{d}l \quad \text{or} \quad k[\mathrm{m}^{-1}] = 0.2998 \, l \, \frac{g[\mathrm{T/m}]}{p[\mathrm{GeV/c}]} \tag{2}$$

where l is the quadrupole length, g the field gradient in the quadrupole, e the particle charge and p the particle momentum. For the parameters given in Tab. 1 the quadrupole strength in (1) corresponds to a magnetic field gradient of

$$0.0055 \, \mathrm{T/m} \leq g \leq 0.055 \, \mathrm{T/m}. \tag{3}$$

We use normalized phase space coordinates (x_n, x'_n) according to

$$x_n = \frac{1}{\sqrt{\beta}} x \quad \text{and} \quad x'_n = \frac{1}{\sqrt{\beta}} (\alpha x + \beta x') \tag{4}$$

where (x, x') are the unnormalized transverse phase space coordinates and α and β are the lattice functions.

3

3 Illustration of the Transverse Echo

The left hand side of Fig. 2 shows the horizontal particle distribution in normalized phase space after the initial dipole offset. In unnormalized phase space, the distribution has a rms value of $\sigma = 2.42$ mm at the maximum β-function. The distributions is offset by 9 mm, corresponding to 3.7σ. The right hand side shows the distribution 500 turns later.
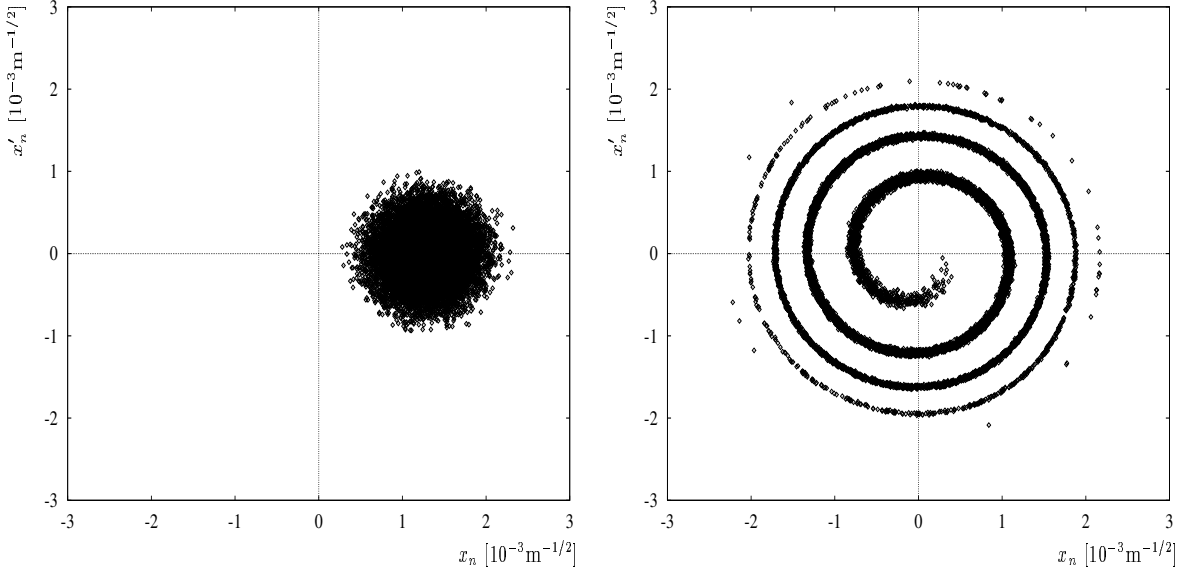

Figure 2: Left: Horizontal particle distribution in normalized phase space after the initial dipole offset. Right: The same distribution 500 turns later.

The left hand side of Fig. 3 shows the particle distribution in normalized phase space right after a one turn long quadrupole kick at turn 500 with $k = 2.0 \cdot 10^{-3} \mathrm{m}^{-1}$. The quadrupole kick results in a deformation of the distribution. The nonlinearity of the transverse oscillation frequency translates the deformation into density modulations along the filaments which rotate in phase space with different frequencies. The right hand side of Fig. 3 shows the distribution 1,000 turns after the initial dipole kick when the high density modulations of the filaments coincide all on the left side of the distribution.

Fig. 4 shows the corresponding dipole signal versus time. The left hand side shows the case of a dipole kick only and the right hand side the case with an additional quadrupole kick. One clearly recognizes the disappearance of the initial dipole signal due to the filamentation in phase space and the reappearance of a dipole moment for the case with the quadrupole kick. The dipole moment reappears at a time $T^* = 2T$ after the dipole kick, where T is the number of turns between the dipole and the quadrupole kick.
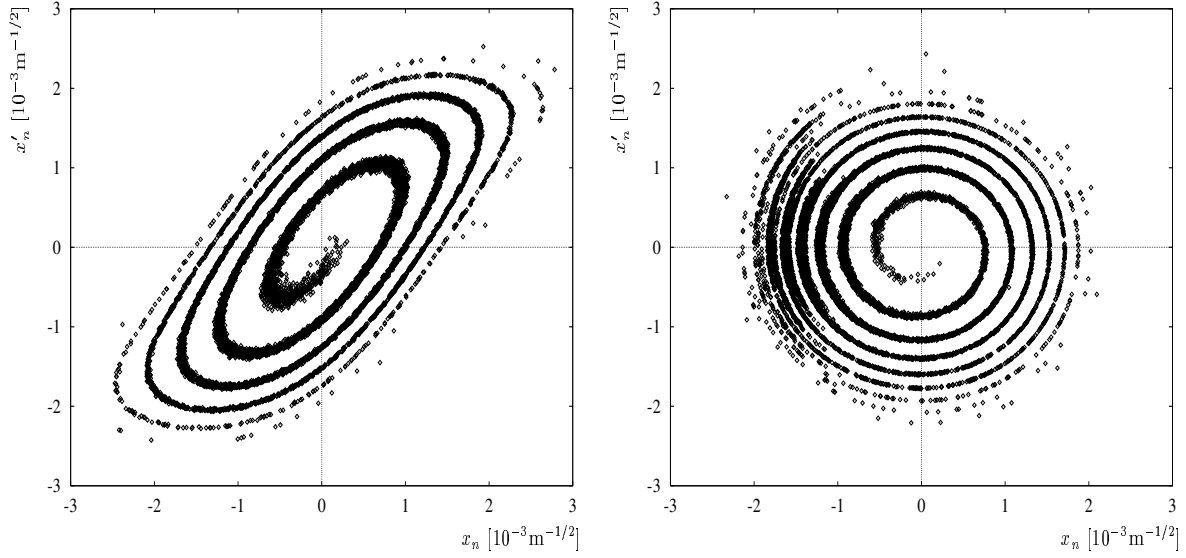
4

Figure 3: Left: Horizontal particle distribution in normalized phase space right after a 1 turn long quadrupole kick placed 500 turns after the dipole kick. Right: The same distribution 500 turns after the quadrupole kick.
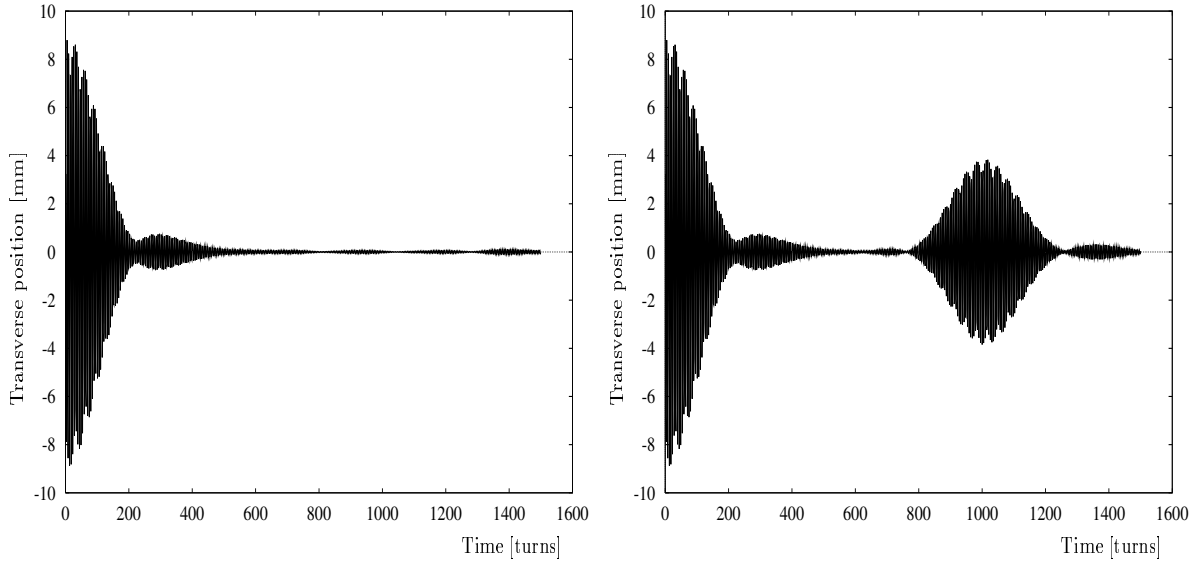

Figure 4: Left: The dipole moment of the distribution versus time after a dipole kick. Right: The same signal with an additional quadrupole kick at 500 turns after the dipole kick.

4 Simulation Results

4.1 Pulsed Quadrupole Excitation

The aim of this section is to determine the maximum acceptable kick length of a pulsed quadrupole kick, the optimum time T between dipole and quadrupole kick and the minimum required kick amplitude. In all cases we assume that the quadrupole signal increases over half the kick length (ramp-up) reaches its maximum signal at half the kick length and decreases again during the second half of the kick length (ramp-down).

The left hand side of Fig. 5 shows such an excitation versus time. The right hand side of Fig. 5 shows the maximum echo response (dipole signal) versus the excitation time ΔT for a quadrupole kick 5,000 turns after the dipole offset with an amplitude of $k = 1.0 \cdot 10^{-3} \mathrm{m}^{-1}$. The signal decreases rapidly for a pulsed excitation which is longer than 10 turns.
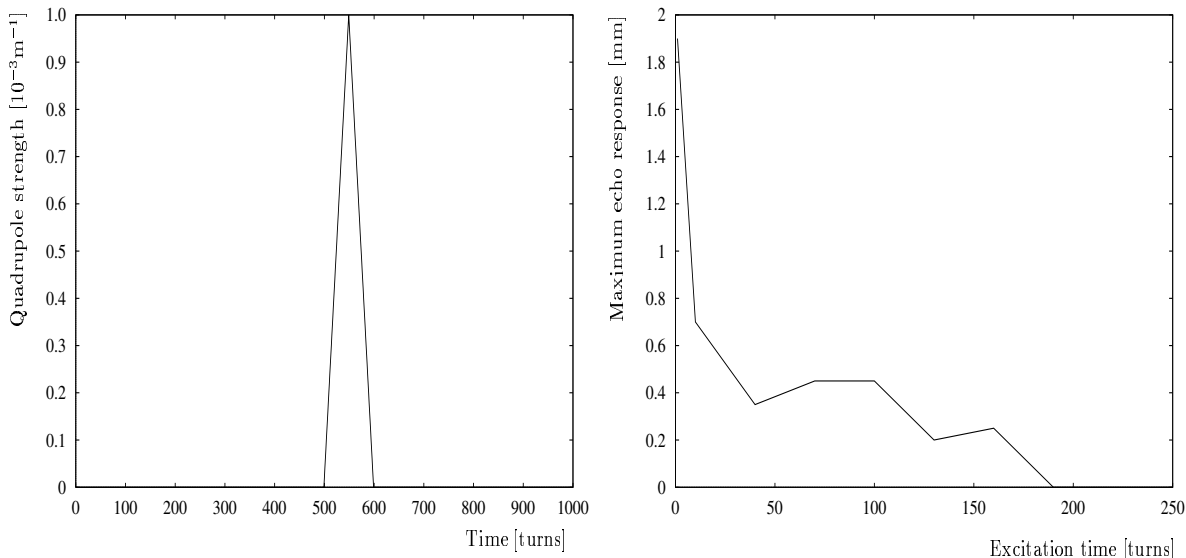

Figure 5: Left: The quadrupole excitation versus time for a amplitude of $k = 1.0 \cdot 10^{-3} \mathrm{m}^{-1}$ and an excitation time of 100 turns. Right: The maximum echo response versus the excitation time ΔT.

Because the particle distribution rotates in the transverse phase space with the betatron frequency a long quadrupole excitation does not lead to a simple elongation and tilt of the phase space distribution but rather to a perturbation which looks approximately uniform over the azimuthal angle of the transverse phase space. Since the echo signal relies on local density deformation along the azimuthal angle of the transverse phase space this uniformity of the distribution reduces the final echo amplitude. For a perfectly uniform azimuthal perturbation of the transverse distribution the echo signal vanishes entirely.

The left hand side of Fig. 6 shows the maximum echo response versus the time separation T between the initial dipole offset and a 10 turn long quadrupole kick with $k = 1.0 \cdot 10^{-3} \mathrm{m}^{-1}$. The echo signal has a maximum amplitude of 5.2 mm for a time

separation of 60,000 turns between the dipole kick and the quadrupole kick. Assuming that the maximum echo response varies linearly with the quadrupole excitation amplitude and requiring a maximum echo response of at least 1/10 of the initial 9 mm dipole signal one needs a quadrupole kick of

$$k \geq 1.8 \cdot 10^{-4} \mathrm{m}^{-1} \ \text{ and } \ \Delta T \leq 10 \text{ turns.} \tag{5}$$

The right hand side of Fig. 6 shows the dipole signal of the distribution versus the number of turns for a 10 turn long quadrupole kick with $k = 1.0 \cdot 10^{-3} \mathrm{m}^{-1}$ at turn 50,000 after the initial dipole offset.
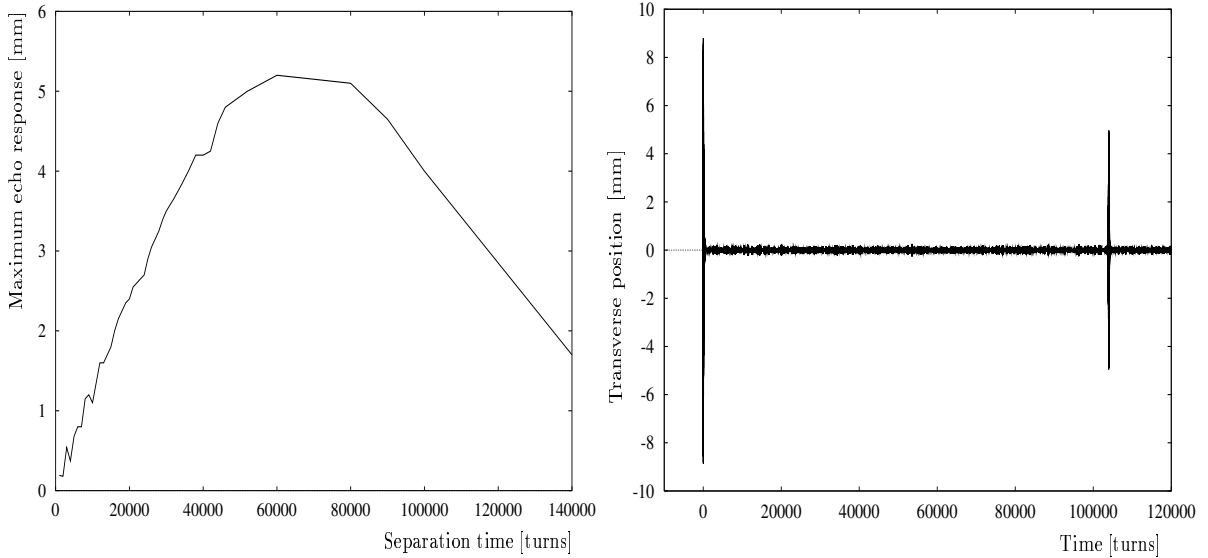

Figure 6: Left: The maximum echo response versus the separation time T between the initial dipole kick and a 10 turn long quadrupole kick with $k = 1.0 \cdot 10^{-3} \mathrm{m}^{-1}$. Right: The dipole signal of the distribution versus time for a 10 turn long pulsed quadrupole kick with $k = 1.0 \cdot 10^{-3} \mathrm{m}^{-1}$ at turn 50,000 after the initial dipole offset.

4.2   AC Quadrupole Excitation

In order to tolerate longer quadrupole excitation times we consider an AC quadrupole signal. The echo signal relies on local density deformations along the azimuthal angle of the transverse phase space. To avoid a spread of the quadrupole kick over different azimuthal orientations of the transverse distribution, we modulate the quadrupole signal with an integer multiple of the betatron frequency.
We consider two cases:

- An AC excitation with twice the betatron frequency. Here, the quadrupole excitation has the same polarity every half rotation of the distribution in phase space and subsequent quadrupole kicks add up coherently.

7

- An AC excitation with the betatron frequency. Here, the quadrupole excitation changes the polarity every half rotation of the distribution in phase space and subsequent quadrupole kicks add up destructively. For a perfectly linear machine the net effect of the kick on the distribution is zero. However, a residual effect remains due to the nonlinearity of the transverse motion which changes the oscillation frequency with amplitude. As a result, consecutive kicks do not cancel perfectly and a residual net deformation remains.

In all cases we assume that the signal envelope of the quadrupole excitation increases over half the kick length (ramp-up) reaches its maximum signal at half the kick length and decreases again during the second half of the kick length (ramp-down).

4.2.1 Modulation with Twice the Betatron Frequency

The left hand side of Fig. 7 shows the AC quadrupole signal for a 240 turn long excitation and a maximum quadrupole amplitude of $k = 1.0 \cdot 10^{-3} \mathrm{m}^{-1}$. The right hand side of Fig. 7 shows the dipole moment of the distribution versus time for a 240 turn long AC quadrupole excitation 5,000 turns after the initial dipole kick and with a maximum quadrupole strength of $k = 2.5 \cdot 10^{-5} \mathrm{m}^{-1}$.
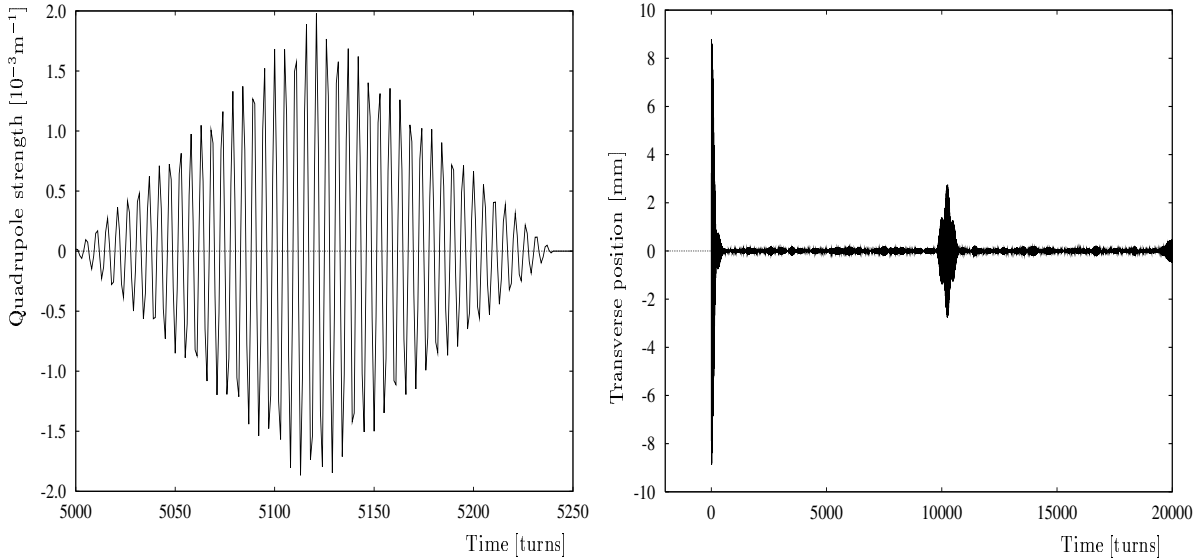

Figure 7: Left: The AC quadrupole strength for a 240 turn long excitation and a maximum quadrupole amplitude of $k = 1.0 \cdot 10^{-3} \mathrm{m}^{-1}$. Right: The dipole moment of the distribution with a 240 turn long AC quadrupole excitation 5,000 turns after the initial dipole offset and with a maximum quadrupole strength of $k = 2.5 \cdot 10^{-5} \mathrm{m}^{-1}$.

Fig. 8 shows the maximum echo response for a 240 turn long quadrupole excitation 5,000 turns after the initial dipole offset versus the maximum quadrupole amplitude. One clearly recognizes the narrow amplitude regime for which one can observe appreciable echo amplitudes. For small quadrupole amplitudes the echo signal diminishes due to the small
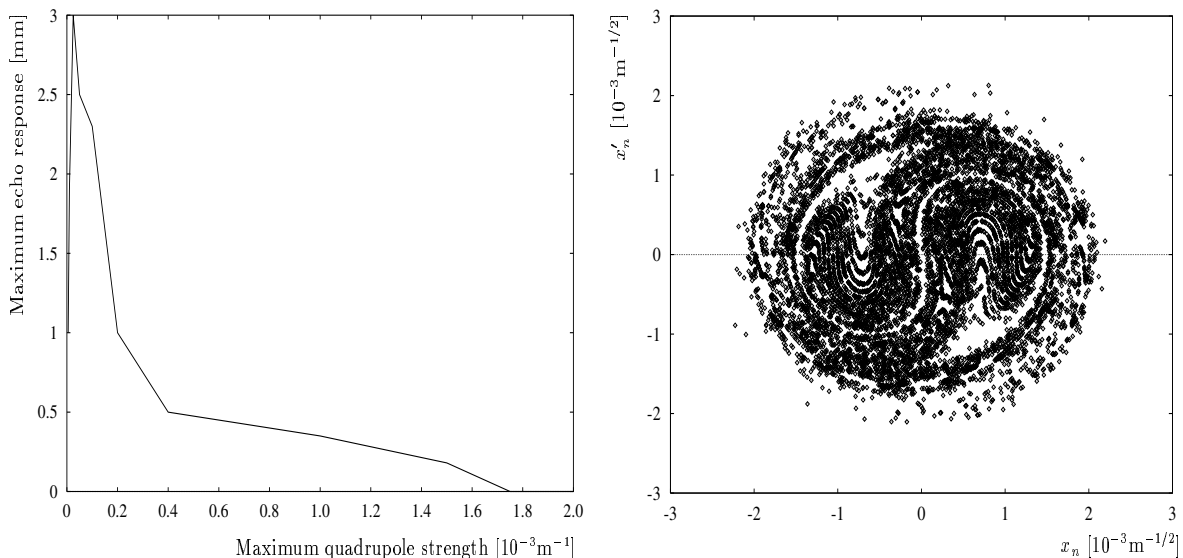
Figure 8: Left: The maximum echo response versus the maximum AC quadrupole amplitude for a 240 turn long excitation 5,000 turns after the initial dipole offset modulated at twice the betatron frequency. Right: The horizontal phase space distribution after a 240 turn long AC quadrupole excitation 5,000 turns after the initial dipole offset and with a maximum quadrupole strength of $k = 2.0 \cdot 10^{-3} \mathrm{m}^{-1}$.

deformation of the transverse phase space and becomes zero for a vanishing quadrupole excitation. For large quadrupole excitations the situation is more complex. Driving the distribution with twice the betatron frequency results in a parametric resonance which changes the topology of the transverse phase space [11]. The right hand side of Fig. 8 shows the horizontal phase space distribution after a 240 turn long AC quadrupole excitation 5,000 turns after the initial dipole offset and with a maximum quadrupole strength of $k = 2.0 \cdot 10^{-3} \mathrm{m}^{-1}$, modulated with twice the betatron frequency. One clearly recognizes the appearance of two new islands left and right from the originally stable fixed point at the center of the phase space. The phase space distortion due to the new islands perturbs the arrangement of density modulations along the dipole filaments which one obtains without the parametric resonance and destroys the final echo signal. Thus, a quadrupole excitation with twice the betatron frequency provides only a narrow amplitude range in which one can observe significant echo amplitudes.

One way of avoiding the phase space deformation due to the parametric resonance it to choose a modulation frequency which is slightly larger than twice the betatron frequency. The drawback of this approach is that the subsequent quadrupole kicks will not exactly add up coherently. Fig. 9 shows the maximum echo response versus the excitation tune for a 240 turn long AC quadrupole excitation 5,000 turns after the initial dipole offset with a maximum amplitude of $k = 1.0 \cdot 10^{-3} \mathrm{m}^{-1}$. While the echo signal almost vanishes for twice the betatron tune ($2Q_x = 0.38$) it achieves significant amplitudes when the modulation tune is increased by approximately 10 %. However, the echo response has several maxima and small changes in the modulation tune or the betatron tune can
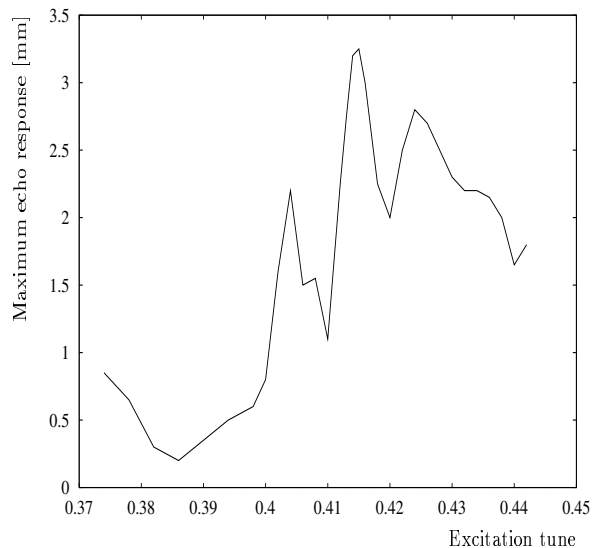
9

Figure 9: The maximum echo response versus the excitation tune ($f_{excitation}/f_{rev}$) for a 240 turn long AC quadrupole excitation 5,000 turns after the initial dipole offset with a maximum quadrupole strength of $k = 1.0 \cdot 10^{-3} \mathrm{m}^{-1}$. The linear horizontal betatron tune is $Q_x = 0.19$.

shift the echo response away from a maximum. Thus, a quadrupole excitation with a frequency slightly larger then twice the betatron frequency provides a sufficiently wide range of excitation amplitudes but an analysis of the echo response requires a careful measurement of the maximum echo response versus modulation frequency.

4.2.2   Modulation with the Betatron Frequency

The left hand side of Fig. 10 shows the maximum echo response for a 240 turn long quadrupole excitation modulated with the betatron frequency and a maximum amplitude of $k = 1.0 \cdot 10^{-3} \mathrm{m}^{-1}$ versus the separation time T between the initial dipole offset and the quadrupole excitation. The echo response follows a Bessel function like modulation similar to the case of a longitudinal echo in a coasting beam [6]. The right hand side of Fig. 10 shows the dipole moment of the distribution versus time for a 240 turn long AC quadrupole excitation 5,000 turns after the initial dipole offset and with a maximum quadrupole strength of $k = 1.0 \cdot 10^{-3} \mathrm{m}^{-1}$.

The left hand side of Fig. 11 shows the maximum echo response for a 240 turn long quadrupole excitation 5,000 turns after the initial dipole offset versus the maximum quadrupole amplitude. Compared to the case of a modulation with twice the betatron frequency the echo response shows a rather wide range of efficient excitation amplitudes. The reason for this is that the topology of the parametric resonance is different from the case of a modulation with the betatron frequency [12]. The right hand side of Fig. 11 shows the horizontal phase space distribution after a 240 turn long AC quadrupole excitation 5,000 turns after the initial dipole offset and with a maximum quadrupole strength
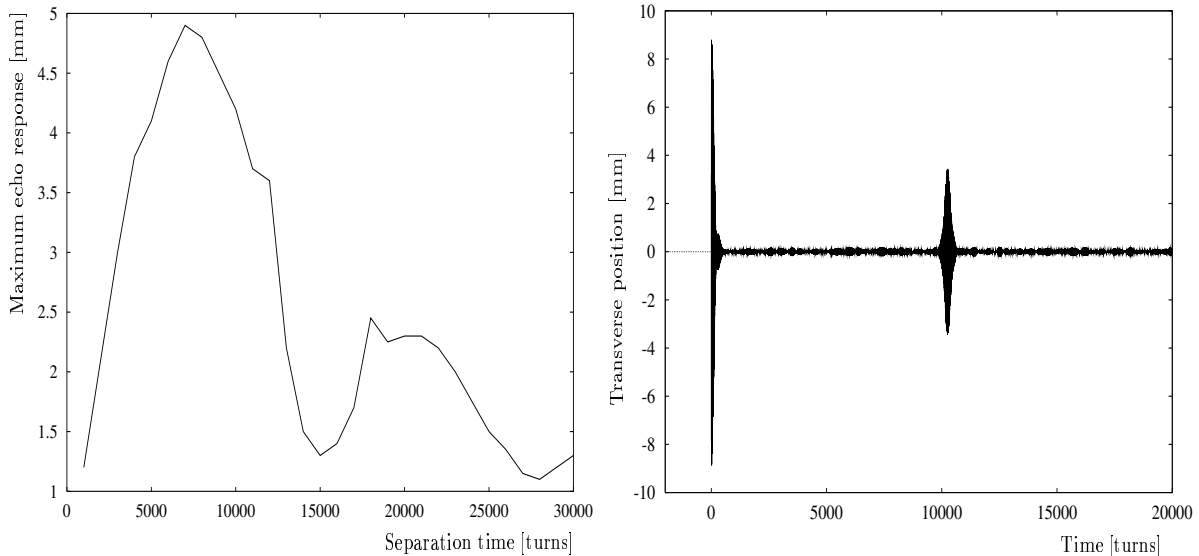
10

Figure 10: Left: The maximum echo response versus the separation time T between the initial dipole offset and a 240 turn long quadrupole excitation modulated with the betatron frequency and a maximum amplitude of $k = 1.0 \cdot 10^{-3} \mathrm{m}^{-1}$. Right: The dipole moment of the distribution with a 240 turn long AC quadrupole excitation 5,000 turns after the initial dipole offset and with a maximum quadrupole strength of $k = 1.0 \cdot 10^{-5} \mathrm{m}^{-1}$ modulated with the horizontal betatron frequency.

of $k = 5.0 \cdot 10^{-3} \mathrm{m}^{-1}$. One clearly recognizes the appearance of a new island around the originally stable fixed point at the center of the phase space.

The left hand side of Fig. 12 shows the horizontal phase space distribution after a 240 turn long AC quadrupole excitation 5,000 turns after the initial dipole offset and with a maximum quadrupole strength of $k = 1.0 \cdot 10^{-3} \mathrm{m}^{-1}$. For $k \leq 2.0 \cdot 10^{-2} \mathrm{m}^{-1}$ the phase space distortions are small and do not perturb much the arrangement of density modulations along the dipole filaments which lead the echo response. Thus, a quadrupole excitation modulated with the betatron frequency provides a large amplitude range for which one can observe significant echo amplitudes. The right hand side of Fig. 12 shows the maximum echo response versus the excitation tune for a 240 turn long AC quadrupole excitation 5,000 turns after the initial dipole offset with a maximum amplitude of $k = 1.0 \cdot 10^{-3} \mathrm{m}^{-1}$. The echo signal peaks for a modulation tune equal to the betatron tune and vanishes for modulation frequencies which differ by more than 10% of the betatron frequency.

The left hand side of Fig. 13 shows the maximum echo response versus the quadrupole excitation time ΔT. For excitation lengths long compared to the filamentation time the echo signal decreases with increasing excitation time. (For the parameters in Tab. 1 the filamentation time corresponds to approximately 250 turns.) However, an excitation time between 50 and 250 turns results in significant echo amplitudes. The right hand side of Fig. 13 shows the maximum echo response versus the detuning with amplitude for a 240 turn long AC quadrupole excitation 5,000 turns after the initial dipole offset with a maximum amplitude $k = 1.0 \cdot 10^{-3} \mathrm{m}^{-1}$.
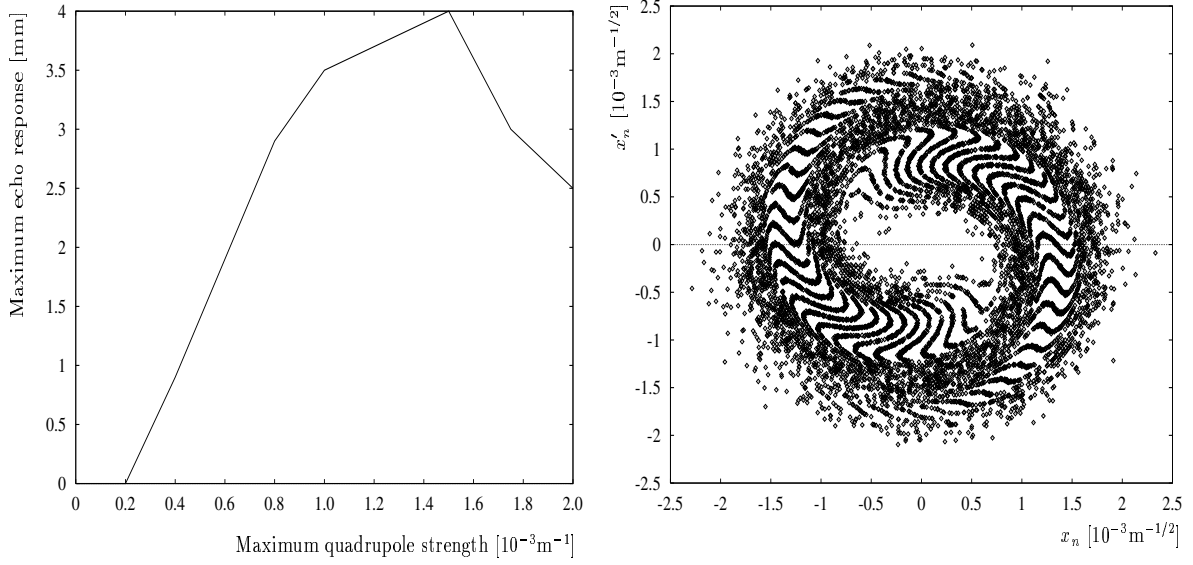
11

Figure 11: Left: The maximum echo response versus the maximum AC quadrupole amplitude for a 240 turn long excitation 5,000 turns after the initial dipole offset and modulated with the betatron frequency. Right: The horizontal phase space distribution after a 240 turn long AC quadrupole excitation 5,000 turns after the initial dipole offset and with a maximum quadrupole strength of $k = 5.0 \cdot 10^{-3} \mathrm{m}^{-1}$.
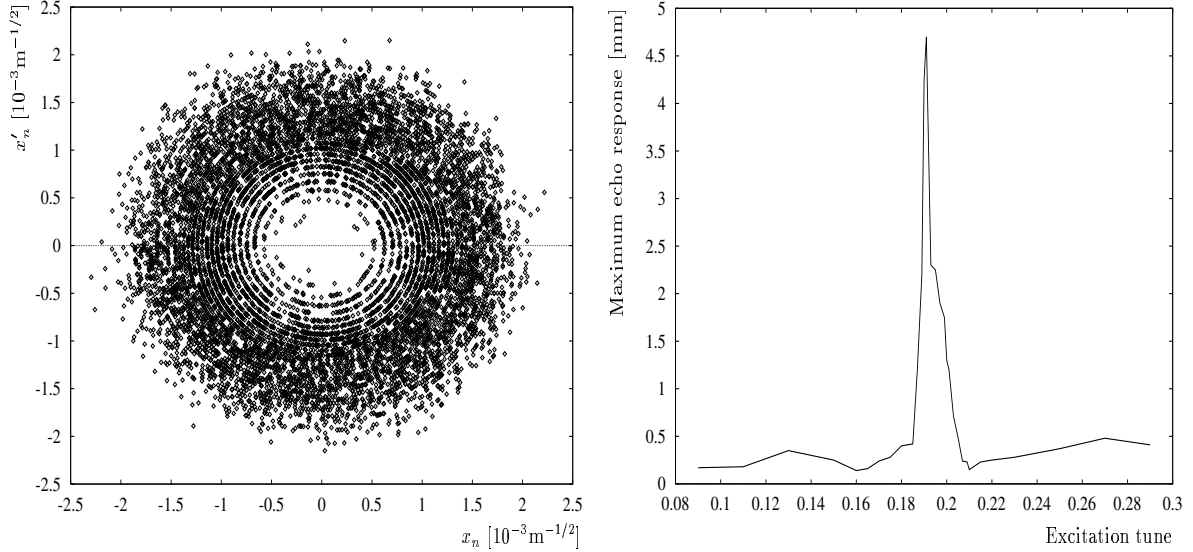

Figure 12: Left: The horizontal phase space distribution after a 240 turn long AC quadrupole excitation 5,000 turns after the initial dipole offset and with a maximum quadrupole strength of $k = 1.0 \cdot 10^{-3} \mathrm{m}^{-1}$. Right: The maximum echo response versus the excitation tune ($f_{excitation}/f_{rev}$) for a 240 turn long AC quadrupole excitation 5,000 turns after the initial dipole offset with a maximum amplitude $k = 1.0 \cdot 10^{-3 \mathrm{m}^{-1}}$. The linear horizontal betatron tune is $Q_x = 0.19$.

The detuning with amplitude changes the filamentation time and results in a similar change of the echo amplitude as a variation of the excitation time. For an excitation length of 240 turns one finds a rather large range of values for the detuning with amplitude which result in significant echo signals.
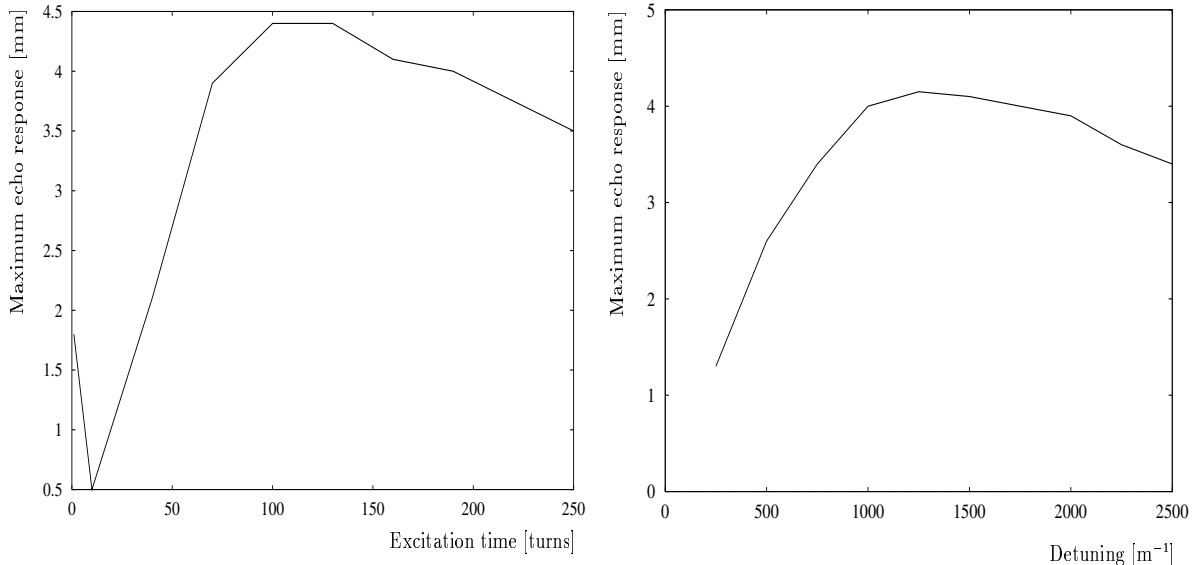

Figure 13: Left: The maximum echo response versus the quadrupole excitation time for an AC quadrupole excitation 5,000 turns after the initial dipole offset and with a maximum quadrupole strength of $k = 1.0 \cdot 10^{-3} \mathrm{m}^{-1}$ modulated with the betatron frequency. Right: The maximum echo response versus the detuning with amplitude for a 240 turn long AC quadrupole excitation 5,000 turns after the initial dipole offset with a maximum amplitude of $k = 1.0 \cdot 10^{-3} \mathrm{m}^{-1}$ modulated with the betatron frequency. The linear horizontal betatron tune is $Q_x = 0.19$.

We investigated whether linear coupling has a significant effect on the echo response. The left hand side of Fig. 14 shows the horizontal and vertical FFT signal of the transverse motion with linear coupling assuming a minimum tune separation of $|Q_x - Q_y| \approx 5 \cdot 10^{-3}$. This is in line with expectations for RHIC. The right hand side of Fig. 14 shows the maximum echo response versus the excitation tune ($f_{excitation}/f_{rev}$) for a 240 turn long AC quadrupole excitation 5,000 turns after the initial dipole offset with a maximum amplitude of $k = 1.0 \cdot 10^{-3} \mathrm{m}^{-1}$ including the linear coupling. This should be compared with Fig. 12.

To model diffusion we introduce random kicks every turn according to

$$\Delta x'_n = D \ \exp\left\{-\sqrt{(x_n^2 + y_n^2)/2}/\sigma\right\} \times r \tag{6}$$

where D is a diffusion coefficient, σ the rms of the particle distribution in normalized phase space and r a random variable out of a normalized Gaussian distribution.
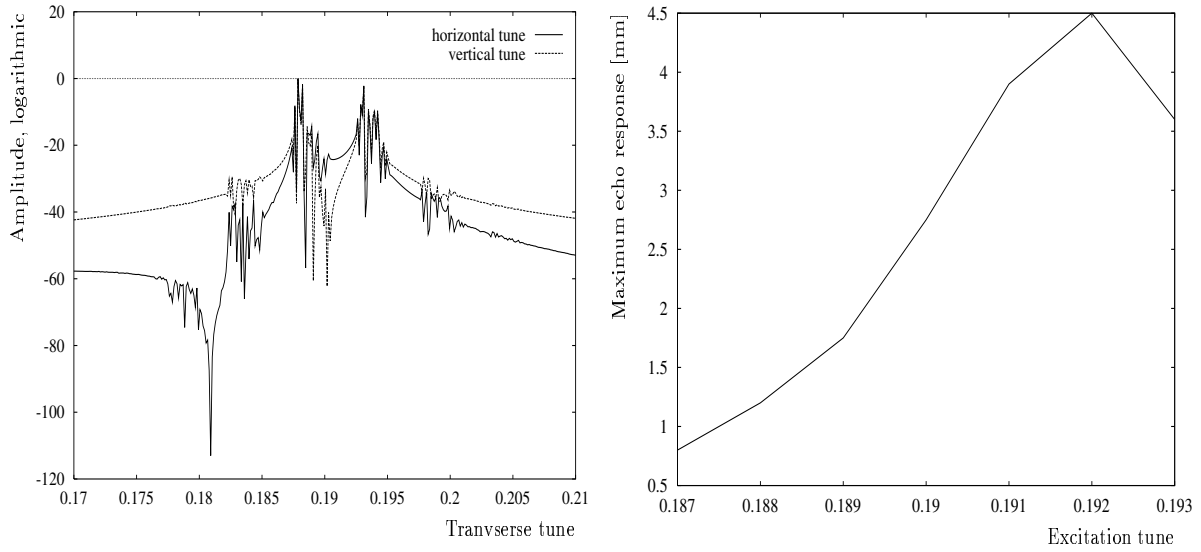
Figure 14: Left: The horizontal and vertical FFT signal of the transverse motion with linear coupling ($|Q_x - Q_y| \approx 5 \cdot 10^{-3}$). Right: The maximum echo response versus the excitation tune ($f_{excitation}/f_{rev}$) for a 240 turn long AC quadrupole excitation 5,000 turns after the initial dipole offset with a maximum amplitude of $k = 1.0 \cdot 10^{-3} \mathrm{m}^{-1}$ and linear coupling ($|Q_x - Q_y| \approx 5 \cdot 10^{-3}$). The linear horizontal betatron tune is $Q_x = 0.19$.
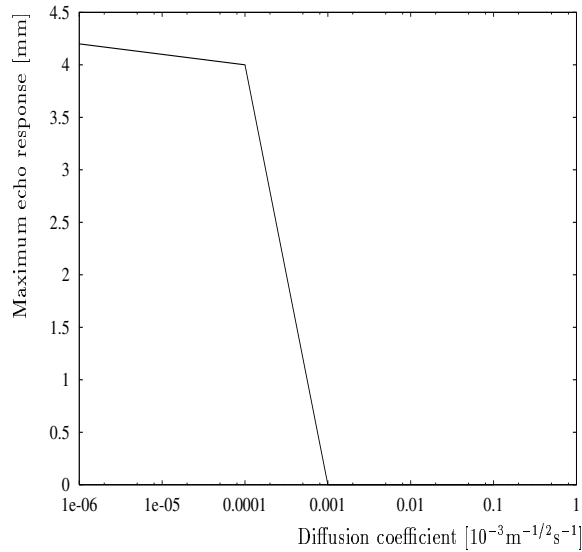

Figure 15: The maximum echo response versus the diffusion coefficient for a 240 turn long AC quadrupole excitation 5,000 turns after the dipole kick with a maximum amplitude of $k = 1.0 \cdot 10^{-3} \mathrm{m}^{-1}$.

The exponential term leads to larger diffusion in regions with high particle density. This is similar to the diffusion process from intrabeam scattering which we expect to be the dominant diffusion source. Fig. 15 shows the maximum echo response as a function of the diffusion coefficient. For diffusion coefficients smaller than $1.0 \cdot 10^{-7} \text{m}^{-1/2}\text{s}^{-1}$ no degradation of the echo response is expected. We expect the diffusion coefficient from intrabeam scattering not to exceed $1.0 \cdot 10^{-8} \text{m}^{-1/2}\text{s}^{-1}$ [13]. To measure this diffusion coefficient the time between quadrupole and dipole kick can be increased.

5 Kickers in RHIC

In this section the possibilities of applying dipole and quadrupole kicks in RHIC are explored. There are several dipole kickers installed in RHIC which may be used in echo type experiments. The challenge lies, however, in the quadrupole kicker. We will investigate whether a quadrupole already installed in RHIC [18], driven by an appropriate power supply, can create a quadrupole kick needed to create an echo signal. As in the simulations we will consider two modes for the quadrupole kicker:

- A pulsed quadrupole excitation of at least 1 turn but no longer than 10 turns.
- An AC-quadrupole excitation over a couple of hundred turns.

5.1 Dipole Kickers

In RHIC there are three types of dipole kickers available: the injection kickers [14,15], the tune kickers [16] and the abort kickers [17]. Their properties are summarized in Tab. 2.

The injection kickers can provide a kick of several σ (see Tab. 2). They are, however, limited to the vertical plane and difficult to operate at low excitation levels. The available range does fit the kick strength assumed in the simulations (3.7σ).

The tune kickers are too weak to provide a single turn dipole kick of sufficient strength. It is conceivable to operate the tune kickers in a multi-turn mode such that subsequent kicks will not cancel out. But the time needed to create the equivalent of a 4σ kick would be in the order of 100 turns, which is already comparable to the filamentation time. While it is likely that the resulting distribution still allows for the detection of a transverse echo signal, the analysis of the signal will be much more complicated than in the case of a single turn dipole kick. The tune kickers would, however, offer the possibility to explore the horizontal plane.

Another possibility to kick in the horizontal plane is to use the abort kickers. But to create a 4σ kick only one of the five kicker magnets must be fired at the lowest possible excitation. Operating the abort kickers in this mode will make it difficult to maintain their function as abort kickers. This may be acceptable during a controlled single bunch experiment at injection energy. The kick length of the abort kickers exceeds one turn which will again result in a complicated particle distribution in phase space after the dipole kick.

We think that the injection kickers are the best choice for the dipole kick. Their limitation to the vertical plane is no principal obstacle for an experiment that aims at showing the possibility of observing transverse echos.

Table 2: RHIC dipole kickers at injection energy.

Kicker	Strength range		Kick length	Kick plane
Injection	0.3–1.5 mrad	4.7–23.5σ_y	60 ns	vertical
Tune (hor)	0–11 μrad	0–0.2σ_x	90 ns	horizontal
Tune (ver)	0–11 μrad	0–0.1σ_y	90 ns	vertical
Abort	0.25–25 mrad	4.2–390σ_x	> 12 μs	horizontal

5.2 Quadrupole Kicker

The quadrupole kicker is the real challenge in producing transverse echos. In the simulations we investigated pulsed quadrupole kicks ranging from 1 to 10 turns and kicks provided by an AC quadrupole over of a couple of hundred turns. We will now estimate the technical feasibility of both approaches.

In both cases we assume that a special air core quadrupole [18] currently installed at IP4 in RHIC and common to both rings will be used to provide the quadrupole kick. This magnet has been designed for a maximum current of 50 A corresponding to a normalized strength of $k = 1.8 \cdot 10^{-3} \text{m}^{-1}$. With the vertical β-function at the magnet location ($\beta_y = 10m$) this is equivalent to $k = 0.4 \cdot 10^{-3} \text{m}^{-1}$ at the maximum β-function in the arcs (see Tab. 1). For the short operating cycles of not more than a few hundred turns the magnet may be able to take more than 50 A.

Fig. 16 shows resistance and inductance measurements for the quadrupole as function of frequency. In one case it is assumed that resistance and inductance are in series while in the other case it is assumed that they are in parallel. In the parallel case the inductance is relatively constant at 125 μH up to a frequency of 1 kHz and drops to about 105 μH at a frequencies beyond 1 kHz.
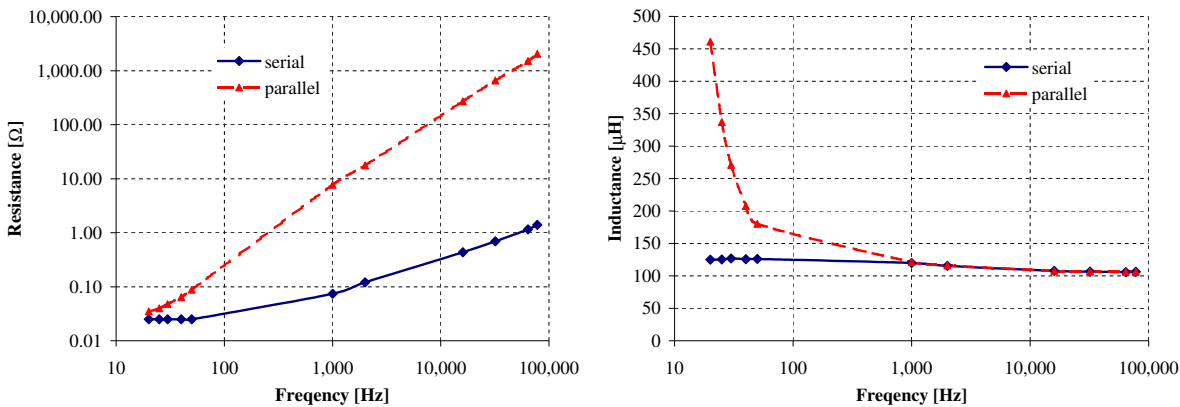

Figure 16: Left: Resistance measurements of the quadrupole. Right: Inductance measurement of the quadrupole. Results with subscript 's' assume that resistance and inductance are in series, results with subscript 'p' assume that resistance and inductance are in parallel.

5.3 A Pulsed Quadrupole Power Supply

A relatively simple design for the pulsed operation of the quadrupole is the one shown in the left hand side of Fig. 17. By closing the switch $S1$ a power supply charges the capacitor C. When charged the swich $S1$ opens again. By closing the switch $S2$ at the time t_0 the capacitor C will start to discharge over the quadrupole with the inductance $L = 125\ \mu$H. We neglect for the moment magnet and cable resistance as well as switching time.
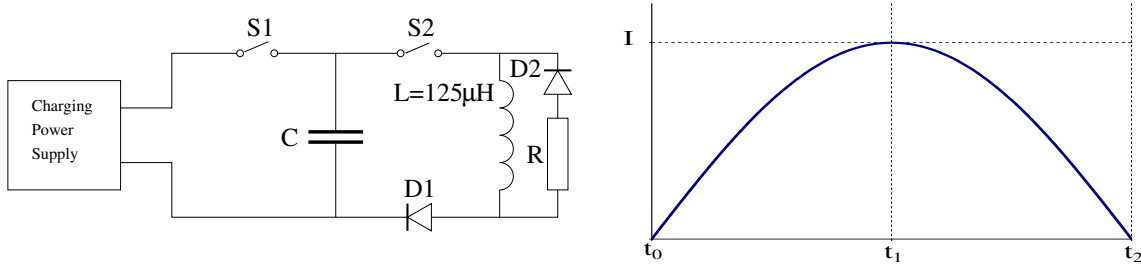

Figure 17: Left: Electric circuit for a pulsed quadrupole. Right: Current in the coil L after the switch $S2$ is closed.

The current in the coil L reaches a maximum after the time t_1 when the switch S2 can be opened again. The energy stored in the coil is then discharged in the resistor R. By choosing R appropriately the current in the coil can be zero after the time t_2 with little further oscillation. During the time $t_2 - t_0$ there is a field in the quadrupole that would create a quadrupole kick. Our simulations showed that the quadrupole kick should be at least one turn but not longer than 10 turns. The time $t_2 - t_0$ can therefore be 2 to 11 turns long (during one turn at the beginning or end of the interval $t_2 - t_0$ there can be a field in the q uadrupole that will not affect the beam).

For the circular frequency ω_0 of the electric circuit, the capacitance C and the voltage V over the coil L the relations

$$\omega_0 = \frac{2\pi}{2(t_2 - t_0)}, \quad C = \frac{1}{\omega_0^2 L} \quad \text{and} \quad V = \omega_0 L I. \tag{7}$$

hold. Fig. 18 shows the capacitance C and the voltage V as a function of the quadrupole kick length assuming that the peak current I_{max} in the coil is 50 A. According to Eq. (7) the voltage over the quadrupole will increase proportionally with the current, which is proportional to the quadrupole kick strength.

5.4 An AC Quadrupole Power Supply

In this approach we try to use the power supply which has been originally built for the quadrupole [18, 19]. This power supply is designed to deliver 50 A at 50 V up to a frequency of 2 kHz. Fig. 19 shows the electric circuit of this solution.
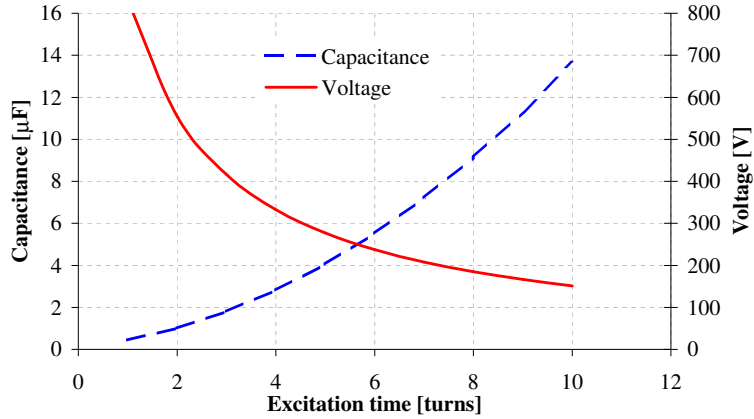
17

Figure 18: Capacitance and voltage as a function of the quadrupole excitation time for a peak current of 50 A in the quadrupole.
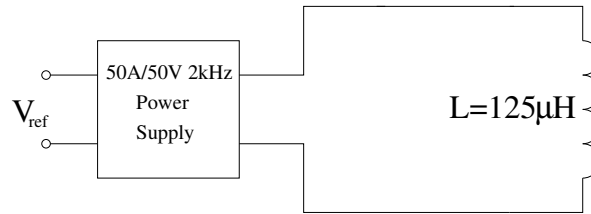

Figure 19: Electric circuit for an AC quadrupole.

The left hand side of Fig. 20 shows the reference voltage of the power supply. A simple step function to the maximum value ensures that the maximum current is reached in the shortest possible time. The right hand side shows the envelope function for the current amplitude in the resonant circuit. As in the simulations, the resonance frequency should be either the β-tron frequency or twice the β-tron frequency. However, the frequency range of that power supply does not match our requirement of either the betatron or twice the betatron frequency. A completely new power supply would need to be designed, a task that appears to be much more challenging than the pulsed power supply solution.
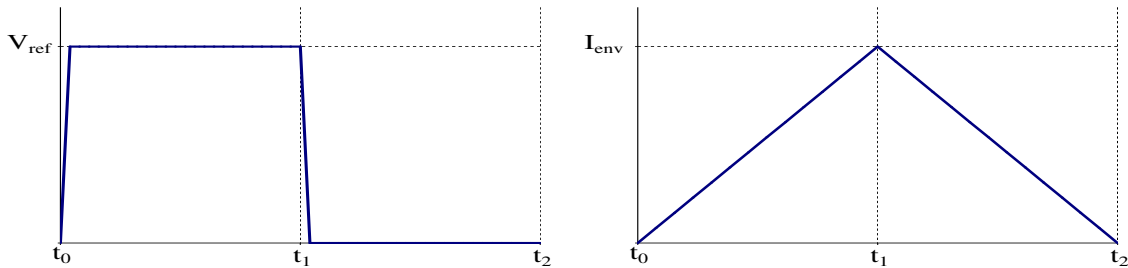

Figure 20: Left: Reference voltage for the AC power supply. Right: Current envelope function of the quadrupole.

18

6 Beam Observation in RHIC

For the observation of transverse echos only beam position monitors (BPMs) are needed. The RHIC arc BPMs are located at positions where the β-function reaches a local maximum (48m). This is the β-function at which we made observations in the simulations. The arc BPMs have a resolution of 0.1 mm if there are more than 10^9 charges per bunch [20]. For protons this is about 1% of the design intensity [9]. The detection of echo signals of several millimeters should therefore pose no problem.

During the RHIC commissioning a turn-by-turn ionization profile monitor (IPM) has been tested successfully [21]. While the BPMs can only detect the center of charge, the IPM would give the projection of the phase space distribution onto the x- or y-axis.

7 Conclusion

From the simulations and the evaluation of the technical possibilities we conclude that it should be possible to observe transverse echos in RHIC. We expect the most promising experimental setup to be:

- RHIC at injection energy with a single bunch of protons
- A vertical dipole kick of about 4σ provided by the injection kicker
- A one-turn quadrupole kick provided by a special air core quadrupole with a maximum current of 50 A
- A separation between dipole and quadrupole kick of about 60,000 turns (0.7 s)
- Echo signal detection with standard arc BPMs in turn-by-turn mode
- Additional observation by the turn-by-turn ionization profile monitor

The main effort needed to realize a transverse echo experiment must concentrate on the construction of a pulsed quadrupole power supply.

References

[1] T.M. O'Neil and R.W. Gould, Phys. Fluids **11**, 1 (1968).

[2] G. Stupakov, "Echo effect in hadron colliders", SSCL-579 (1992).

[3] G. Stupakov and S. Kauffmann, "Echo effect in accelerators", SSCL-587 (1992).

[4] N. Mahale et al., "Displaced bunch synchrotron oscillation echoes in accelerators", SSCL-N-817 (1993).

[5] L.K. Spentzouris, J.-F. Ostiguy and P.L. Colestock, "Direct measurement of diffusion rates in high energy synchrotrons using longitudinal beam echoes", PRL Vol. 76, No 4, pp. 620 (1996).

[6] O. Brüning, "On the possibility of measuring longitudinal echos in the SPS", CERN SL/95-83 (AP) (1995).

[7] O. Brüning et al., "Beam echos in the CERN SPS", proceedings of the 1997 Particle Accelerator Conference, Vancouver, (1997).

[8] J. Kewisch and M. Brennan, "Bunched beam echos in the AGS", proceedings of the 1998 European Particle Accelerator Conference, Stockholm (1998).

[9] "RHIC Design Manual", revision of April 1998.

[10] D. Lie et al., "Effects of rf voltage modulation on particle motion", Nucl. Instr. and Meth. in Phys. A 364 205-223 (1995).

[11] M. Bai et al., "Adiabatic excitation of longitudinal bunch shape oscillations", proceedings of the 1999 Particle Accelerator Conference, New York (1999).

[12] O. Brüning, "An analysis of the long-term stability of the particle dynamics in hadron storage rings", PhD thesis, DESY 94-085 (1994).

[13] W. Fischer et al., "Emittance growth in RHIC during injection", proceedings of the LHC96 Workshop on High Brightness Beams for Large Hadron Colliders, Particle Accelerators Vol. 58, Numbers 1-4 and BNL RHIC/AP/112 (1996)

[14] W. Fischer et al., "Beam Injection into RHIC", proceedings of the 1997 Particle Accelerator Conference, Vancouver (1997).

[15] H. Hahn, J.E. Tuozzolo, "The RHIC injection kicker", proceedings of the 1997 Particle Accelerator Conference, Vancouver (1997).

[16] P. Cameron et al.,"ARTUS: A Rhic TUne monitor System", BNL RHIC/AP/156 (1998).

[17] H. Hahn et al., "The RHIC Beam Abort Kicker System", proceedings of the 1999 Particle Accelerator Conference, New York, (1999).

[18] W. Fischer, A. Jain and D. Trbojevic, "The AC quadrupole in RHIC", RHIC/AP/164 (1999).

[19] J. Biggs and J. Dinkel, "Bucker quad power supply", private note, 16 May 1991.

[20] P. Cameron and T. Shea, private communication (1999).

[21] P. Cameron et al., "The RHIC Ionization Beam Profile Monitor", proceedings of the 1999 Particle Accelerator Conference, New York, (1999).